International Core Journal of Engineering Volume 7 Issue 5, 2021
ISSN: 2414-1895 DOI: 10.6919/ICJE.202105_7(5).0024

Fractional Order Fuzzy Controller for Load Frequency Control in Ship Microgrid based on Differential Evolution Algorithm

Bo Zheng, Jianmei Xiao and Xihuai Wang

Logistics Engineering College, Shanghai Maritime University, Shanghai 201306, China.

Abstract

The imbalance of the active power in ship microgrid will cause the system frequency fluctuation. To stabilize the microgrid frequency fluctuation, a fractional order fuzzy control parameter optimizing scheme, based on improved differential evolution algorithm, is proposed. The basic idea of the proposed method is formulating the optimal design issue of the controller as a typical constrained optimization problem. On the basis of the fractional PID controller with fuzzy logic control, and the system parameters are optimized by an improved differential evolution algorithm. The simulation results show that the controller combined with fuzzy logic has better anti-interference performance, and the improved differential evolution algorithm has faster convergence speed and higher convergence accuracy. In an environment where load power and renewable energy power are unstable, the proposed method this method has better frequency suppression and robustness.

Keywords

Load Frequency Control; Ship Microgrid; Fractional PID; Fuzzy Control; Differential Evolution Algorithm.

1. Introduction

The non-renewability of petroleum resources, air pollution and greenhouse effect have made people turn their attention to renewable energy [1]. The introduction of wind and solar energy into the ship's power system to form a hybrid electric propulsion system has become an important direction for ship research. However, when the ship is sailing, it is subject to uncertain disturbances such as wind, waves and sunlight. For example, wind power generation is affected by wind speed and wind direction, and photovoltaic power generation is affected by solar light intensity and solar radiating angle, which will lead to the imbalance between the output power and load power of the ship microgrid, and eventually cause the frequency fluctuation of the grid. When the frequency fluctuation of the power grid exceeds a certain range, it will bring hidden dangers to the safe navigation of ships. Therefore, in order to ensure the safety of ship navigation, it has important practical significance to carry out research on the load frequency control of ship microgrid.

For the problem of Load Frequency Control (LFC), relevant scholars have conducted a lot of research. A robust controller is designed based on the principle of H_∞ mixed sensitivity, and linear matrix inequality method is used to solve it in [2], the results show that this method can improve the robust stability of the ship's power system. A power system load frequency control based on the MPC algorithm, is given in [3], and the simulation showed that the stability and speed are better than the PI algorithm. The model predictive control based on neural network is investigated in [4].

In recent years, with the continuous development of artificial intelligence technology, artificial neural networks, genetic algorithms, and fuzzy technology have been widely used in the field of microgrid load frequency control. In [5], the elephant group nomadic optimization algorithm is used to design

ISSN: 2414-1895 DOI: 10.6919/ICJE.202105_7(5).0024

the load frequency controller. In [6], the differential evolution algorithm is applied to the load frequency control system of the multi-source power system, and the simulation results show that the algorithm has a better effect on optimizing parameters. In [7-9], the application of improved differential evolution algorithm is presented in their respective fields.

When the above control scheme involves the PID control part, the order of the controller is integer order. In order to further improve the effect of ship microgrid load frequency control, a fractional order fuzzy control (PCFDE) parameter optimization scheme based on improved differential evolution algorithm is proposed to achieve the purpose of suppressing frequency oscillation of ship power grid system. The simulation results show that under the environment of load disturbance and renewable energy power disturbance, the proposed scheme has good dynamic performance and robustness to suppress the frequency fluctuation of ship microgrid.

2. Establishment of the microgrid model

The marine microgrid power system is generally composed of diesel generator (Diesel Generator, DG), flywheel energy storage system (Flywheel), energy storage battery (Battery), photovoltaic power generation system (Photovoltaic, PV), wind turbine power generation system (Wind Turbine, WT) and electric load (Load). Diesel generators bear the main output power as traditional power generation equipment. Since the power generated by renewable energy sources such as solar and wind energy depends on weather conditions, there is a lot of uncertainty. The fluctuation of load power and renewable energy output power will be compensated by increasing or decreasing the output power of diesel generators and charging and discharging energy storage batteries, so as to achieve a dynamic balance of power supply and demand. The power balance of the system satisfies the following formula [10]

$$\Delta P_l = \Delta P_{pv} + \Delta P_w + \Delta P_g \pm \Delta P_b \tag{1}$$

Where, P_l is the load power, P_{pv} is photovoltaic power, P_w is the output power of wind turbine, P_g diesel generator output power, P_b is the exchange power of energy storage battery.

The form of linearized equation of synchronous generator rotor motion

$$\begin{cases} M\frac{d\omega}{dt} = \Delta P - D\Delta\omega \\ \frac{d\Delta\delta}{dt} = \Delta\omega \end{cases} \tag{2}$$

Where, M is the inertial coefficient, D is the damping coefficient, δ is the electrical angular velocity, ω is the rotational speed. For (2) Laplace transform has

$$Ms\Delta\omega(s) = \Delta P(s) - D\Delta\omega(s) \tag{3}$$

It can be further expressed as

$$\frac{\Delta f(s)}{\Delta P(s)} = \frac{1}{Ms+D} \tag{4}$$

The diesel generator set is composed of prime mover, generator and governor. The governor controls the prime mover power by controlling the valve switch, which can be expressed as

$$\Delta X_d(s) = \frac{1}{T_d s+1}\left[\Delta u_c - \frac{1}{R}\Delta f(s)\right] \tag{5}$$

Where, ΔX_d is the governor output; T_d is the governor time constant, Δu_c is the system input; R is the adjustment coefficient.

The prime mover converts chemical energy into kinetic energy output and drives the generator to do work to output electrical energy. Its movement process can be expressed as a first-order inertia link

$$\frac{\Delta P_g(s)}{\Delta X_d(s)} = \frac{1}{T_g s+1} \tag{6}$$

Where, T_g represents the prime mover time constant.

ISSN: 2414-1895 DOI: 10.6919/ICJE.202105_7(5).0024

As an auxiliary energy source, the energy storage battery ignores the effects of temperature and aging internal resistance changes, and its dynamic process

$$\frac{\Delta P_{\mathrm{b}}}{\Delta f}=\frac{1}{T_{\mathrm{b}}\,s+1} \tag{7}$$

The load frequency control model of the microgrid is shown in Figure 1 below.

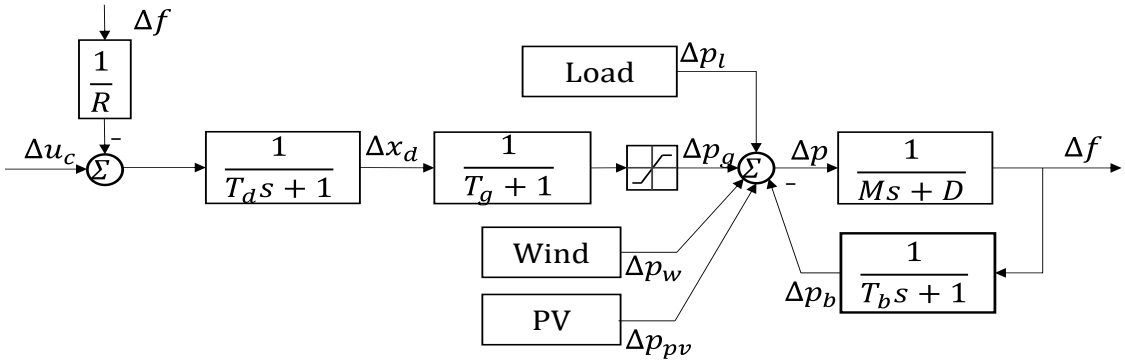

Figure 1. Schematic diagram of micro-grid LFC system model

In Figure 1, Δu_c is the controller output signal; Δf is the system frequency deviation; Δu_d is the governor output signal; T_d is the governor time constant; T_g is the prime mover time constant; T_b is the energy storage battery time constant; M is the power system inertia coefficient; D is the power system damping coefficient; R is the adjustment coefficient.

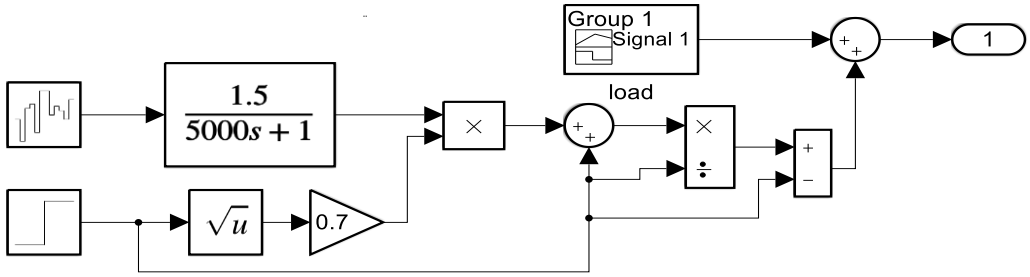

(a) Load model

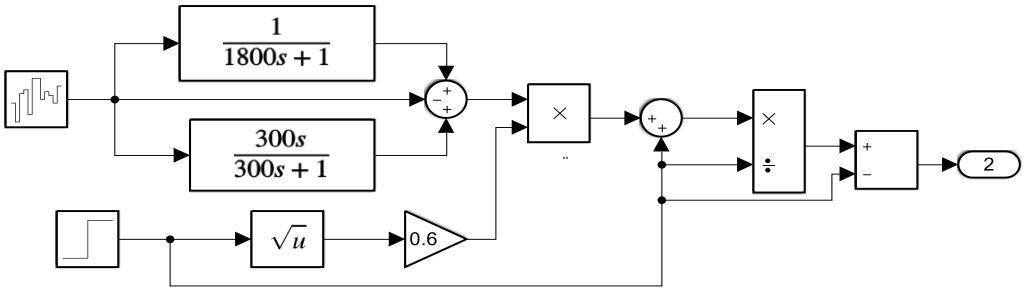

(b) Wind power model

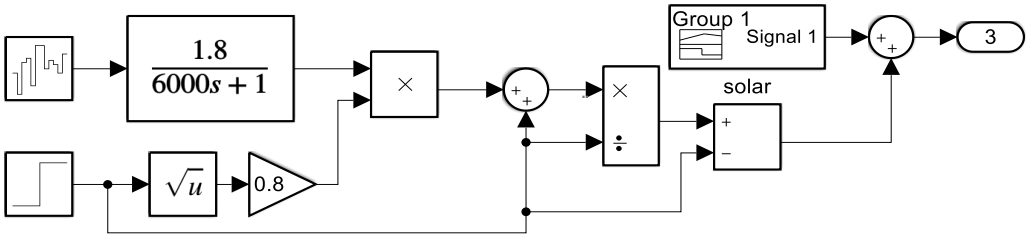

(c) Photovoltaic power generation model

Figure 2. Load, wind and PV power generation models

ISSN: 2414-1895 DOI: 10.6919/ICJE.202105_7(5).0024

Due to the uncertainty of wind speed and direction, sunlight intensity and angle, and sudden changes in user load, the output power of wind power generation system and photovoltaic power generation system is unstable, the output power deviation of load, wind power and photovoltaic power generation is shown in Figure 2.

3. Controller design

3.1 Fractional Calculus Theory

Fractional calculus is a generalization of integral calculus. The basic operation operator of fractional calculus is ${}_aD_t^\alpha$, as shown in equation (8).

$$ {}_aD_t^\alpha = \begin{cases} \frac{d^\alpha}{dt^\alpha} & \alpha > 0 \\ 1 & \alpha = 0 \\ \int_a^t d\tau^{-\alpha} & \alpha < 0 \end{cases} \tag{8} $$

Where, a and t are the upper and lower limits of the operator, and α is the order of calculus. The most commonly used definitions of fractional calculus are Riemann-Liouville (RL) definition and Grunwald-Letnikov (GL) definition.

RL is defined as

$$ {}_aD_t^\alpha f(t) = \frac{1}{\Gamma(m-\alpha)} \frac{d}{dt}^m \int_a^t \frac{f(\tau)}{(t-\tau)^{1-(m-\alpha)}} d\tau \tag{9} $$

Where, m-1<α<m, and Γ(z) is the Euler Gamma function.

$$ \Gamma(z) = \int_0^\infty e^{-t} t^{z-1} dt \tag{10} $$

GL is defined as

$$ {}_aD_t^\alpha f(t) = \lim_{h\to 0} \frac{1}{\Gamma(\alpha) h^\alpha} \sum_{k=0}^{(t-a)/h} \frac{\Gamma(k+\alpha)}{\Gamma(k+1)} f(t-kh) \tag{11} $$

Under the initial condition of 0, the Laplace transform of differential order n (n > 0) is transformed into

$$ L\{D^n x(t)\} = s^n X(s) \tag{12} $$

The transfer function of the fractional control system based on the theory of fractional calculus is

$$ G(s) = \frac{a_m s^{\alpha m} + a_{m-1} s^{\alpha m-1} + \cdots + a_0 s^{\alpha_0}}{b_n s^{\beta n} + a_{n-1} s^{\beta n-1} + \cdots + b_0 s^{\beta_0}} \tag{13} $$

Where, $(a_m, b_n) \in \mathbb{R}^2, (\alpha_m, \beta_n) \in \mathbb{R}_+^2, \forall m, n \in N$.

3.2 Fractional controller

The general form of the fractional PID controller is $PI^\lambda D^\mu$ controller, and the form of the transfer function is

$$ G(s) = K_p + \frac{K_i}{s^\lambda} + K_d s^\mu \ \ (\lambda, \mu) \in \mathbb{R}_+^2 \tag{14} $$

Where, λ is the order of the integral; μ is a differential order and its value range in fractional order PID control is [0 2].

For the fractional-order PID controller, when λ=1, μ=0, it is the PI controller; when λ=0, μ=1, it is the PD controller, when λ=1, μ=1, it is the PID Controller. It can be seen that the fractional-order PID controller is a generalization of the integer-order PID controller. Due to the addition of two adjustable parameters, the parameter adjustment range of the fractional-order controller is wider, which can better improve the system performance.

Oustaloup recursive filtering method can fit fractional calculus operators, and the constructed transfer function model of the filter is

ISSN: 2414-1895 DOI: 10.6919/ICJE.202105_7(5).0024

$$G_f(s) = K\prod_{k=1}^{N}\frac{s+\omega_k^{'}}{s+\omega_k} \tag{15}$$

The poles and zeros of the filter can be expressed as

$$\omega_k = \omega_b\left(\frac{\omega_h}{\omega_b}\right)^{\frac{k+N+\frac{1}{2}(1+\gamma)}{2N+1}} \tag{16}$$

$$\omega_k^{'} = \omega_b\left(\frac{\omega_h}{\omega_b}\right)^{\frac{k+N+\frac{1}{2}(1-\gamma)}{2N+1}} \tag{17}$$

$$K = \omega_h^{\gamma} \tag{18}$$

The algorithm parameters, ω_b =0.01, ω_h=100, N=2.

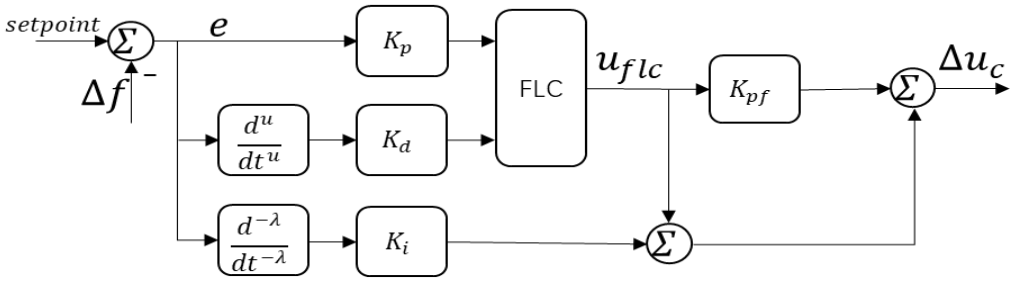

Figure 3. The general scheme of the control

Table 1. The fuzzy rules set

$\dot{e}$	e						
	NL	NM	NS	ZR	PS	PM	PL
PL	ZR	PS	PM	PL	PL	PL	PL
PM	NS	ZR	PS	PM	PL	PL	PL
PS	NM	NS	ZR	PS	PM	PL	PL
ZR	NL	NM	NS	ZR	PS	PM	PL
NS	NL	NL	NM	NS	ZR	PS	PM
NM	NL	NL	NL	NM	NS	ZR	PS
NL	NL	NL	NL	NL	NM	NS	ZR

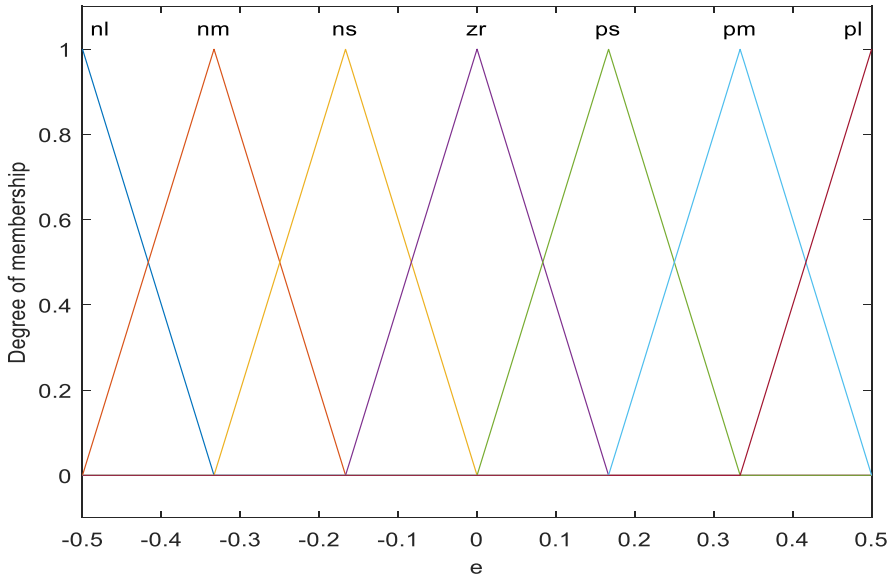

Figure 4. Membership functions for error

ISSN: 2414-1895 DOI: 10.6919/ICJE.202105_7(5).0024

3.3 Fuzzy logic

On the basis of the above section, the fuzzy rules are introduced to further process the proportional and integral signal, and the controller structure is shown in Fig. 3. The basic idea of fuzzy rules is based to the error and its change rate, the controller applies a signal to speed up or slow down the speed close to the set target value. The fuzzy controller is divided into seven levels of fuzzy subsets: {NL}, {NM}, {NS}, {ZR}, {PS}, {PM}, {PL}, corresponding to {negative large}, {negative medium}, {negative small}, {zero}, {positive small}, {positive medium}, {positive large}, respectively. The fuzzy rules are shown in Table 1. The membership function of the error derivative $\dot{e}$ and the membership function of the output signal u_{flc} are consistent with the membership function of the error e. The membership function of the error e is designed as shown in Figure 4.

4. Differential evolution algorithm

4.1 Typical differential evolution algorithm

The differential evolution algorithm (DE) is used to solve the optimal solution in a multidimensional space. It has the advantages of simple structure, fast convergence and easy implementation. The process mainly includes the following four steps:

1 Initialize the population of individuals. Individuals satisfying constraints are randomly generated in n-dimensional space, where, x_{ij}^{U} and x_{ij}^{U} are the upper bounds and lower bounds of the jth individual, respectively. The operation is as follows:

$$x_{ij}(0) = rand(0,1)\left(x_{ij}^{U} - x_{ij}^{L}\right) + x_{ij}^{L} \tag{19}$$

2 Mutation operation. The basic mutation strategy is to randomly select 3 individuals in the population, and $h1 \neq h2 \neq h3$. The formula is as follows, namely

$$h_{ij}(t+1) = x_{h1j}(t) + F\left(x_{h2j}(t) - x_{h3j}(t)\right) \tag{20}$$

Determine whether the value in a certain dimension of h_{ij} is out of bounds. If it is, takes the extreme value, where, F is mutation operation and controls the mutation step size.

3 Cross operation. CR is cross factor and can effectively increase population diversity. Binomial crossover is performed by the following rule:

$$v_{ij}(t+1) = \begin{cases} h_{ij}(t+1) & rand(0,1) \leq CR \\ x_{ij}(t) & rand(0,1) > CR \end{cases} \tag{21}$$

4 Select operation. The individual vector generated after mutation and crossover will be compared with the target vector to determine which vector enters the next generation, $f(x)$ as the objective function, and the operation is

$$x_i(t+1) = \begin{cases} v_i(t+1) & f\left(v_i(t+1)\right) < f\left(x_i(t)\right) \\ x_i(t) & f\left(v_i(t+1)\right) \geq f\left(x_i(t)\right) \end{cases} \tag{22}$$

Repeat step 2 to step 4, until reaching the maximum evolution algebra, or the minimum objective function value.

Typical differential evolution algorithm mutation factor F is 0.9, and cross factor CR is 0.5.

4.2 Improved differential evolution algorithm

The probability of each individual being selected to participate in mutation is proportional to the value of its fitness function. Based on this roulette idea, the basic idea of the differential evolution algorithm based on probability choice of population individuals (PCDE) proposed in this paper is: according to the fitness of each individual, each iteration reorders the whole population individual. The larger the fitness is, the smaller the position sequence number is, and the smaller the fitness is, the larger the position sequence number is. At the same time, the probability of individual being selected is determined according to the position sequence number. The smaller the position sequence number is,

ISSN: 2414-1895 DOI: 10.6919/ICJE.202105_7(5).0024

the smaller the probability of being selected is. the larger the position sequence number is, and the greater the probability of being selected is. In figure 5, P, Fit and SeN refer to population individuals, fitness, and location numbers, respectively.

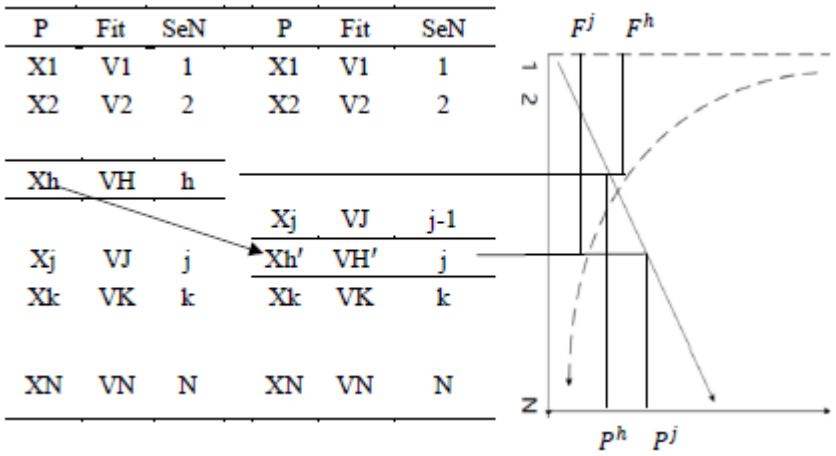

Figure 5. The idea based on probability

In Figure 5, the fitness are sorted from large to small, namely V1>V2>…>VH>…>VJ>VK>…>VN, and the position numbers are sorted from small to large, namely, 1<2<…<h<…<j <k<...<N. The fitness of individual Xh after its nth iteration is VH, the position number is h, the probability of being selected is P^h, and the corresponding mutation factor is F^h. If the fitness of the individual after the n+1th iteration is VH', and satisfies VJ≤VH'≤VK, the position number is j, the probability of being selected is P^j, and the corresponding mutation factor is F^j, If the fitness does not change after n+1th iterations, and remains VH, the position number, the probability of being selected and the corresponding mutation factor remain unchanged. The probability P of the individual being selected in Figure 5 is given by

$$P_h = \frac{\frac{h}{N}}{\sum_1^N \frac{h}{N}} = \frac{2h}{N+N^2} \qquad \text{h=1,2,...,N} \tag{23}$$

Where, h is the position number, N is the population size, and P_h is the probability corresponding to the individual position number h. It can be seen from equation (23) that N is fixed, and the probability P corresponding to each position number h is also fixed. The mutation factor F in Figure 5 is given by

$$F = \frac{1}{3}(\sum_1^3 F^h) \quad \text{h} \in 1,2,...,\text{N} \tag{24}$$

$$F^h = ab^h \quad \text{h} \in 1,2,...,\text{N} \tag{25}$$

Where, h is the position number, and the value range of F^h is [0.7 1.2].

The optimal individual of the probability selection population is defined as the individual with the smallest fitness, and the worst individual is the individual with the largest fitness. In each iteration, the optimal individual and the worst individual are updated. For individuals participating in mutation operation, when the fitness is close to the optimal individual fitness, it will have a greater probability to be selected to participate in mutation operation, and the corresponding mutation factor is small to increase the local search capability. When the fitness is close to the worst individual fitness, it will have a greater probability not to be selected to participate in mutation operation, and the corresponding mutation factor is large to enhance the global search capability.

The optimal individual for the jth update in the population is defined as XN_j, and the worst individual is $X1_j$. The distance between XN_j and $X1_j$ is R_j. H_j is the variation vector after extreme value treatment in Equation (20). The distance between H_j and $X1_j$ is D_j. In order to prevent the cross

ISSN: 2414-1895 DOI: 10.6919/ICJE.202105_7(5).0024

factor CR is too small at the beginning of iteration, and the number of iterations is introduced to limit it, the cross factor CR is expressed as (28), and its initial value is 0.5.

$$R_j = |XN_j - X1_j| \tag{26}$$

$$D_j = |H_j - XN_j| \tag{27}$$

$$cr_j = \begin{cases} cr = 0.3, D_j < \omega_1 R_j \&\& \ t > \omega_2 T \\ cr = 0.5, D_j < \omega_3 R_j \ t > \omega_4 T \\ cr = 0.7, others \end{cases} \tag{28}$$

For equation (28), when the number of iterations is low and the variant individual is far from the global optimal individual and closer to the global worst individual, the crossover factor is set to a larger value to increase the diversity of the population and improve the ability of global search. When the number of iterations is high and the mutated individual is closer to the global optimal individual and far from the global worst individual, the crossover factor is set to a smaller value to reduce the ability of the population diversity to concentrate resources and increase local search. In formula (28), ω_1=0.3, ω_2=0.7, ω_3=0.6, ω_4=0.3, t is the current iteration number, and T is the total iteration number.

4.3 Fitness function design

The purpose of controller parameter optimization is to quickly eliminate the system frequency deviation when the ship microgrid system is disturbed. Time multiplied by the absolute error integral performance index (Integral of Time multiplied Absolute Error, ITAE) is used as the minimum objective function for parameter optimization. In order to avoid the saturation of the actuator caused by the excessive control signal, the Integral of Squared Controller Output (ISCO) is added to the objective function to obtain the objective function of the system as follows

$$MinJ = \int_0^t [\omega_1 t|e(t)| + \omega_2 u^2(t)]dt \tag{29}$$

where, $e(t)$ is the frequency deviation of the microgrid; $u(t)$ is the output signal of the controller; t is the time variable; ω_1 and ω_2 are the corresponding weighting coefficients, which are 10 and 0.1 respectively. On this basis, this paper introduces the maximum fluctuation frequency and the minimum fluctuation frequency

$$MinJ = \int_0^t [\omega_1 t|e(t)| + \omega_2 u^2(t) + \omega_3|\Delta f_{max}\ | + \omega_4|\Delta f_{min}\ |]dt \tag{30}$$

In the formula, Δf_{max} and Δf_{min} are the maximum fluctuation frequency and the minimum fluctuation frequency, respectively, ω_3 and ω_4 are the corresponding weighting coefficients, and the value is 0.1. The constraint condition of formula (30) is that the maximum values of k_p, k_i, k_d, λ, μ, k_{pf} are 100,100,100,1. 5,1. 5,100, and the minimum values are 0.

4.4 Algorithm steps

1 Executive (19) initializing population

2 Calculate the fitness of individual population

3 Selecting the optimal individual and obtaining the optimal fitness

4 Carry out the idea of Figure 5, copy the initial population and update the population probability selection. According to the fitness of population, the individuals are arranged in descending order, and the position number is given.

5 Executive formula (23) calculates the probability of individuals entering the mutation operation according to the position sequence number. Executive formula (24) obtains the mutation factor in formula (20).

6 In the probability selection population, according to the calculation result of (23), select individuals to perform the mutation operation in equation (20), and judge whether the vector h is out of bounds. If it is beyond the bounds, perform the boundary extreme value operation.

ISSN: 2414-1895 DOI: 10.6919/ICJE.202105_7(5).0024

7 Execute formula (28) to select the cross factor, and execute formula (21) to complete the cross operation.

8 Perform the selection operation of Equation (22), return the better individual and its fitness to replace the current value of the initial population as the next generation of the individual.

9 Judge and update, and return the optimal individual of the population and its fitness

10 Judge whether the maximum number of iterations is reached, if not, return to step 4, if it is reached, jump out of the loop, and output the optimal individual and optimal fitness.

5. Simulation example

The load frequency control model of the ship microgrid is built in the Matlab/SIMULINK. The model parameters are shown in Table 2 below. The algorithm population size is 30, and the number of iterations is 70. For other parameters of the algorithm, seen Section 4.1~4.3.

Table 2. Micro-grid model parameters

Symbol	Numerical Value	Symbol	Numerical Value
T_d/s	0.08	R	2.4
T_g/s	0.3	D	0.012
T_b/s	0.1	M	0.2

When the ship is sailing, there is a sudden increase or decrease in power demand such as emergency braking and a sudden increase in the power of electrical equipment. In this case, the load power deviation of the ship's microgrid has the attribute of a step signal, a step disturbance signal of 15%pu. is applied to the system at 1s. Under the action of this signal, the corresponding frequency deviation signal of the marine microgrid is shown in Figure 7. The algorithm optimization results are as follows, the parameter under the DE algorithm, k_p=10.7555, k_i=0.7130, k_d=19.3239, λ=1.2243, μ=1.1093, J=0.1149. The parameter under the PCDE algorithm, k_p=9.3132, k_i=0.7203, k_d=16.9876, λ=1.2676, μ=1.0832, J=0.0761. each parameter value under PCFDE algorithm, k_p=3.6308, k_i=0.2109, k_d=16.3814, λ=1.3174, μ=1.0397, k_{pf}=2.5304, J=0.0754, J is the optimal fitness.

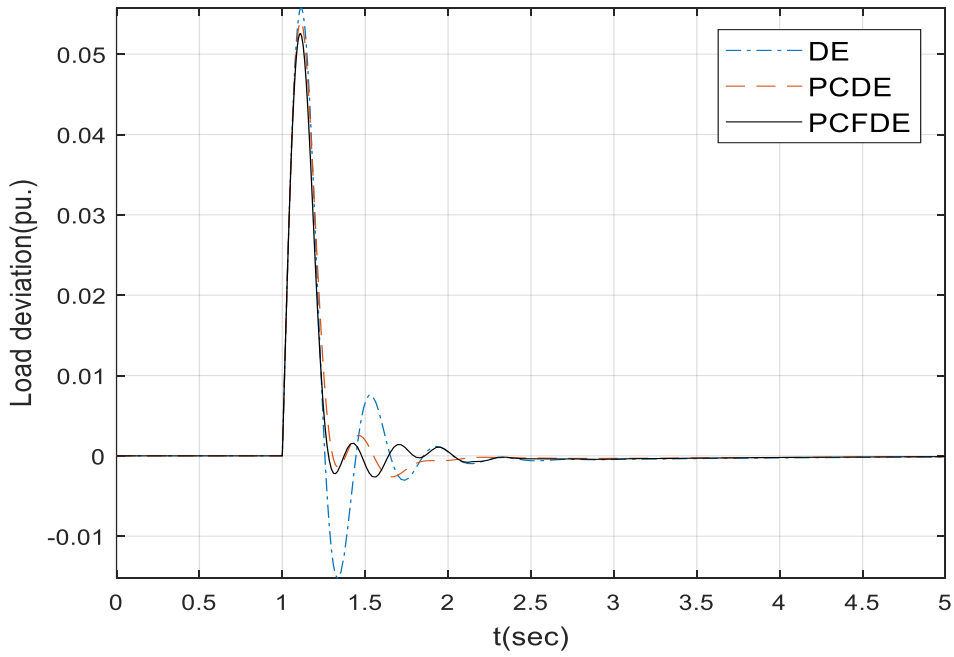

Figure 6. Frequency response by step signal deviation signal

ISSN: 2414-1895 DOI: 10.6919/ICJE.202105_7(5).0024

Table 3. Algorithm comparison data

Algorithm	Max(pu.)	Min(pu.)	T(t)	N	J
DE	0.05575	-0.01525	1.563928	5	0.1149
PCDE	0.05411	-0.00261	1.270684	4	0.0761
PCFDE	0.05282	-0.00264	1.249153	7	0.0754

Processing the image information in Figure 6 yields the data in Table 3, the maximum frequency peak value (Max), minimum wave valley value (Min), adjustment time (T), number of oscillations (N) and optimal fitness (J). It can be clearly seen that the maximum and minimum amplitudes of the improved algorithm are reduced by 0.0016pu. and 0.013pu, respectively, the adjustment time is shortened by 0.3s, the number of oscillations is reduced by one, and the optimal fitness is reduced by 0.0388. After adding fuzzy logic, compared with the improved algorithm, the number of oscillations is increased by 3 times, but several other indicators are further reduced. Compared with the number of oscillations, the frequency overshoot and adjustment time are more worthy of attention. The simulation results prove that the control scheme in this paper can have a better suppression effect on system frequency fluctuation when the ship load power suddenly increases or decreases.

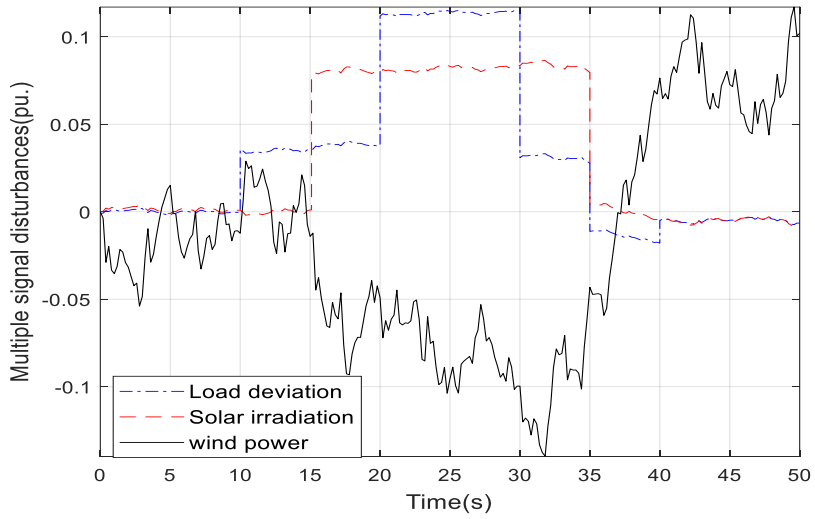

Figure 7. Multi-signal disturbance

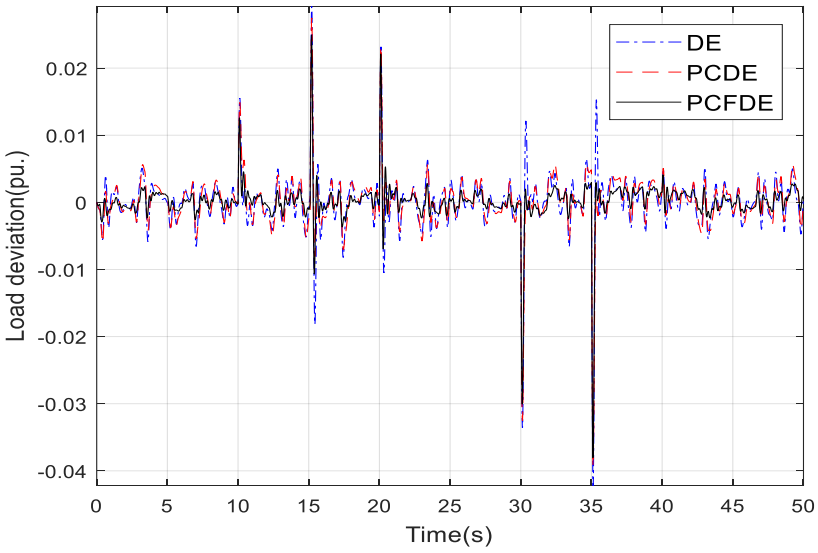

Figure 8. Microgrid frequency

ISSN: 2414-1895 DOI: 10.6919/ICJE.202105_7(5).0024

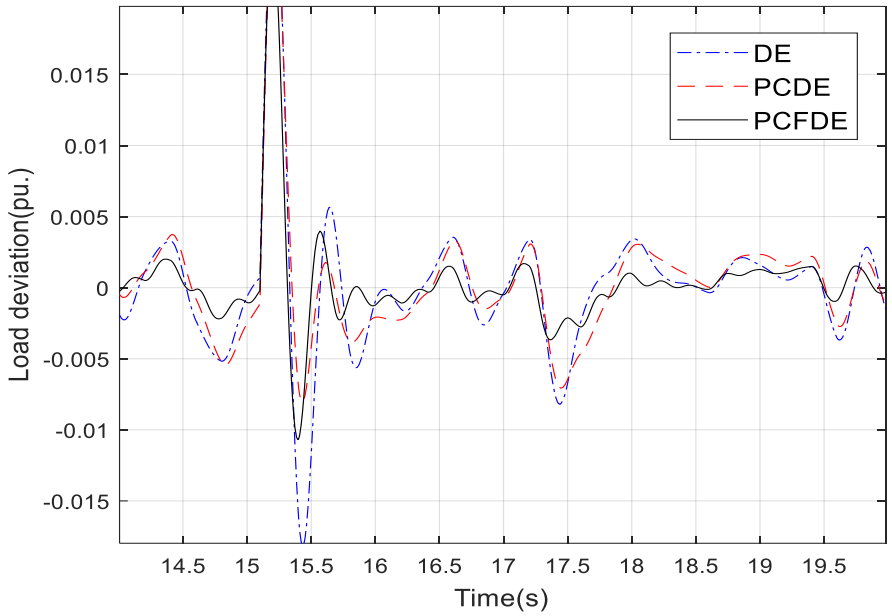

Figure 9. Partially enlarged details

Table 4. Algorithm comparison data

Algorithm	Max(pu.)	Min(pu.)	Va(*E-05)	Am(*E-04)
DE	0.02912	-0.0422	2.8956	28
PCDE	0.02744	-0.0393	2.5506	26
PCFDE	0.02492	-0.0380	1.8706	17

When a ship is sailing, the output power of wind turbines and solar panels depends on the weather conditions during the ship 's voyage. Except for the input signal change, the other parameters are consistent with the parameter settings of the step signal. Figure 7 is the signal output from the simulation of the model in Figure 2, which has the attributes of load frequency disturbance, photovoltaic power generation and wind power generation. Figure 8 is the frequency output of the microgrid under this signal, Figure 9 is a partial enlarged view of Figure 8 between 14s and 20s, and processing the image information in Figure 8 yields the data in Table 5.

Table 4 shows the frequency maximum peak value (Max), minimum valley value (Min), variance (Va) and the average value of the absolute value (Am). It can be seen that the indicators of the improved algorithm are significantly better than the original algorithm, especially after the introduction of fuzzy modules, the indicators are reduced by 0.0042 pu., 0.0042 pu., 1*E-05 and 11*E-04, respectively. It shows that in the face of disturbances such as photovoltaic and wind instability, the control scheme can more effectively ensure the frequency stability of the ship power grid system and ensure the safety of the ship.

Ships cannot avoid the problem of aging failure of power system equipment, and the established mathematical model does not match the real system. When the system parameter T_g is perturbed by 15%, other system parameter settings, input signals and algorithm parameters remain unchanged. The simulation results are shown in Figure 10. processing the image information in Figure 10 yields the data in Table 5, The two indicators in Table 5 are the maximum frequency difference (MaxD) and the average of the absolute value of the frequency difference (MeanD) at the same time when the same algorithm parameter is perturbed by 15%, which are reduced by 6.6 and 2.3 units respectively after improvement. This also illustrates from another perspective that the improved scheme can better maintain the frequency stability of the ship power grid.

ISSN: 2414-1895 DOI: 10.6919/ICJE.202105_7(5).0024

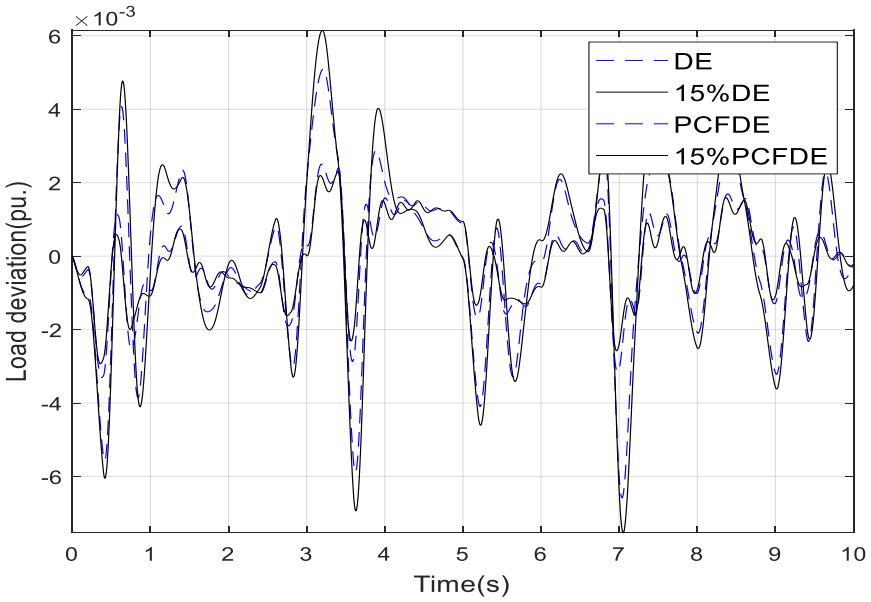

Figure 10. System output response with parameters perturbation

Table 5. Algorithm comparison data

Algorithm	MaxD(pu.*E-04)	MeanD(pu.*E-04)
DE	14.82658	4.02714
PCFDE	8.23730	1.69597

6. Conclusion

For the load frequency control problem of the hybrid ship microgrid, this paper builds a load frequency control model, designs a fractional-order fuzzy control structure, and uses an improved differential evolution algorithm to find the optimal control parameters. And through the example simulation, it is verified that this kind of control scheme has more obvious control effect on the ship microgrid frequency. In the next step, the idea of sliding mode variable structure control will be introduced, which may achieve better anti-interference effects.

References

[1] CHEN J Y, LI X J, XIE W. Microgrid Frequency Control Based on H_∞ Mixed Sensitivity[J]. Power System Technology, 2014, 38(9):2399-2403.

[2] LI H Y, WANG X H, XIAO J M, et al. robust control of load frequency in diesel-battery hybrid electric propulsion ship[J]. Chinese Journal of Ship Research,2017,12(3):120-127.

[3] YANG G, LIU M G, QU Z J. Load frequency control of power systems based on MPC algorithm[J]. Journal of Beijing Jiaotong University, 2012, 36(2):105-110.

[4] KASSEM A M. Neural predictive controller of a two-area load frequency control for interconnected power system[J]. Ain Shams Engineering Journal, 2010, 1(1):49-58.

[5] SAMBARIYA D K, FAGNA R. A robust PID controller for load frequency control of single area re-heat thermal power plant using elephant herding optimization techniques[C]. 2017 International Conference on Information, Communication, Instrumentation and Control (ICICIC), 2017:1-6.

[6] MOHANTY B, PANDA S, HOTA P K. Controller parameters tuning of differential evolution algorithm and its application to load frequency control of multi-source power system[J]. International Journal of Electrical Power & Energy Systems, 2014, 54(1):77-85.

[7] Hong Z, Zhang G J, Adaptive differential evolution algorithm based on Nth-order nearest-neighbor analysis[J]. Control Theory & Applications, 2011(11):1613-1620.

ISSN: 2414-1895 DOI: 10.6919/ICJE.202105_7(5).0024

[8] Han Q C, Zhao Q L. Optimization design of laminates based on improved differential evolution algorithm[J]. Hoisting and Conveying Machinery, 2020, No.549(01):94-97.

[9] Method of Image Recognition for Lepidopteran Insects Based on Improved Differential Evolution Algorithm[J]. Scientia Silvae Sinicae, 2020, v.56(03):76-84.

[10] SRIMANNARAYANA P, BHATTACHARYA A, SHARMA S. Load Frequency Control of Microgrid Considering Renewable Source Uncertainties[C]. 2018 International Conference on Computation of Power, Energy, Information and Communication (ICCPEIC), 2018:419-423.